1

Climate and Environmental Modelling Programme (CEMP)

Capacity to model and forecast climate and environmental processes at different spatio-temporal scales has the potential to revolutionize our approach and ability to address many issues that concern us closely. It was to address these issues in an integrated manner and to generate a capability for multi-scale forecasting that CEMP was initiated.

Highlights

The year 2004-2005 had seen a number of significant developments in CEMP. C-MMACS is now a major participant in a national multi-institutional extended-range monsoon prediction (MI-ERMP) programme, which seeks to improve prediction of monsoon rainfall with a multi-model ensemble. C-MMACS has been also involved in a number of national and international programmes and projects.

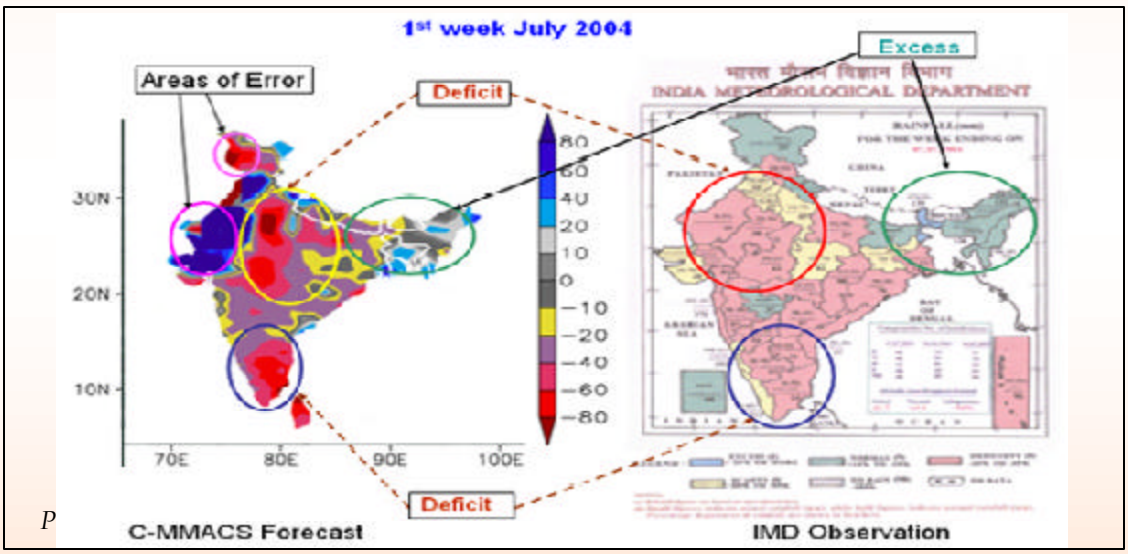

P

Inside

1.1 A Post Forecast Evaluation of C-MMACS Experimental Long-range Monsoon Forecast

The critical to enabling roles that accurate, long-range forecasts of monsoon rainfall can play in areas like agricultural planning can hardly be overemphasized. Such forecasts, especially at spatial resolution comparable to a district (typically 50km x 50 km) remain a major scientific challenge. On the other hand, the requirement at the user level is often for spatial resolution that corresponds to a taluk (typically 10km x 10km), as rainfall shows significant variability at this scale, necessitating a taluk-level agricultural planning. While accurate, long-range forecasts of rainfall at such spatial resolution is not available anywhere in the world at present, the Karnataka State Natural Disaster Monitoring Centre (KSNDMC), Karnataka carried out an exploratory study with the experimental long-range forecasts generated by C-MMACS. C-MMACS has initiated dynamical long-range forecasting of monsoon rainfall in 2003 using a variable-resolution atmospheric general circulation model (VR AGCM). The C-MMACS forecast was one of the very few that accurately predicated the severe drought of 2003 over Karnataka, although 2003 was a normal monsoon at all-India level.

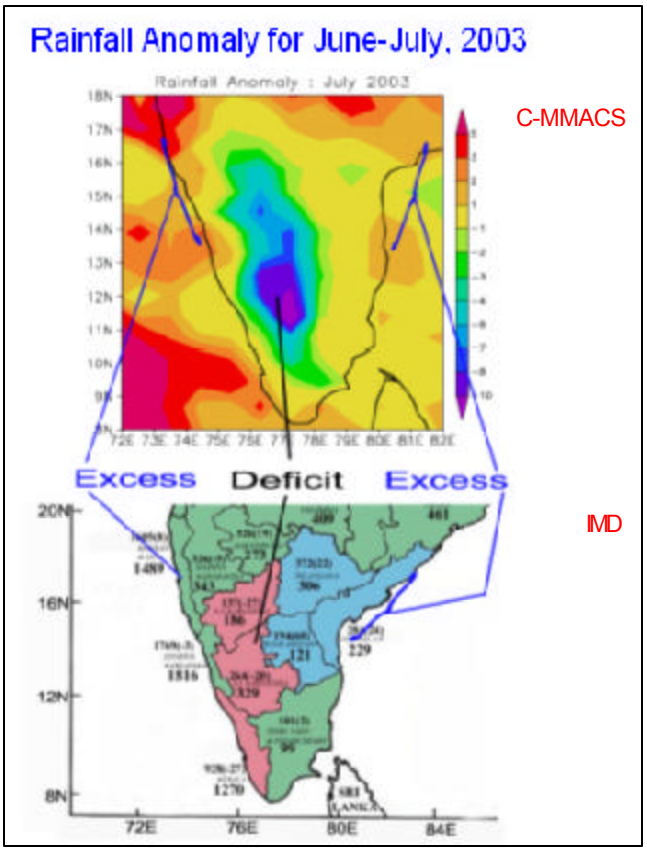

Fig 1.1 A comparison of C-MMACS Experimental long-range forecasts (issued in April 2003) of rainfall with subsequent observations from India Meteorological Department (IMD) over South India.

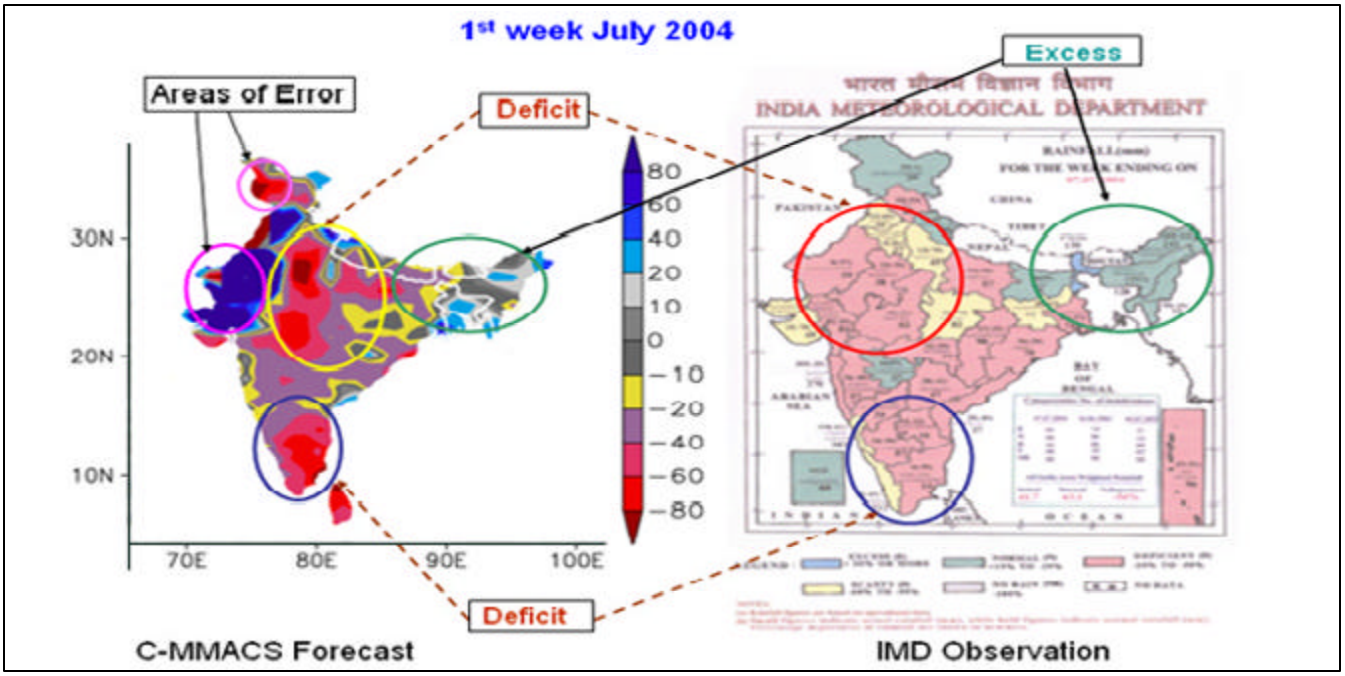

Fig 1.2 A comparison of C-MMACS experimental long-range forecasts of rainfall for the first week of July 2004 with the corresponding observations from India Meteorological Department (IMD). Except for two small areas of error over western and Kashmir sector, the forecasts captured the distribution of rainfall well.

Fig 1.1 shows a comparison of C-MMACS forecast for June-July rainfall 2003 over South India and the corresponding observation from India Meteorological Department (IMD). Encouraged by this success KSNDMC had requested C-MMACS to generate long-range district level forecasts of rainfall for the state of Karnataka for the summer monsoon of 2004 in an experimental mode. Here we present an overview of performance of these forecasts. Although the basic C-MMACS forecasts were at district scale, they were downscaled to taluk level at KSNDMC using a simple procedure. These taluk-level forecasts were then compared with observed rainfall (anomalies) after the end of the season.

The highlight of the methodology is a variable resolution GCM that allows relatively higher resolution (zoom) over a chosen domain. The forecast model is adopted from the variable resolution GCM developed at LMD, France. The version used in the present studies uses a diurnal cycle, a land surface module and convective parameterization scheme of Tidtke. The model grid has 192 x 145 points in the horizontal direction with a zoom over the monsoon domain, which provides a horizontal resolution of about 60 km x 50 km around the zoom which merges smoothly to about 2^o x 2^o away from the zoom. The number of vertical levels is 19. The initial conditions are extracted from daily fields from NCEP available on a 2.5^o x 2.5^o grid. For reasons of numerics, each district was identified as a rectangular box (of approximately 1^ox1^o dimension) characterized by longitudes and latitudes defining the district.

The forecasts were generated through a multi-lead ensemble averaging of nine simulations generated with initial conditions taken for the period April-May 2004. The forecasts were then represented as normalized percentage anomalies with respect to (15-year) model climatology. As an example, Figure 1.2 compares the forecast for first week of July, 2004 with the corresponding observation from IMD. Except two small areas of error over western sector and Kashmir, the forecasts could capture the distribution of anamolies quite well.

To quantify the performance of the forecast at taluk level, we have used the following measure

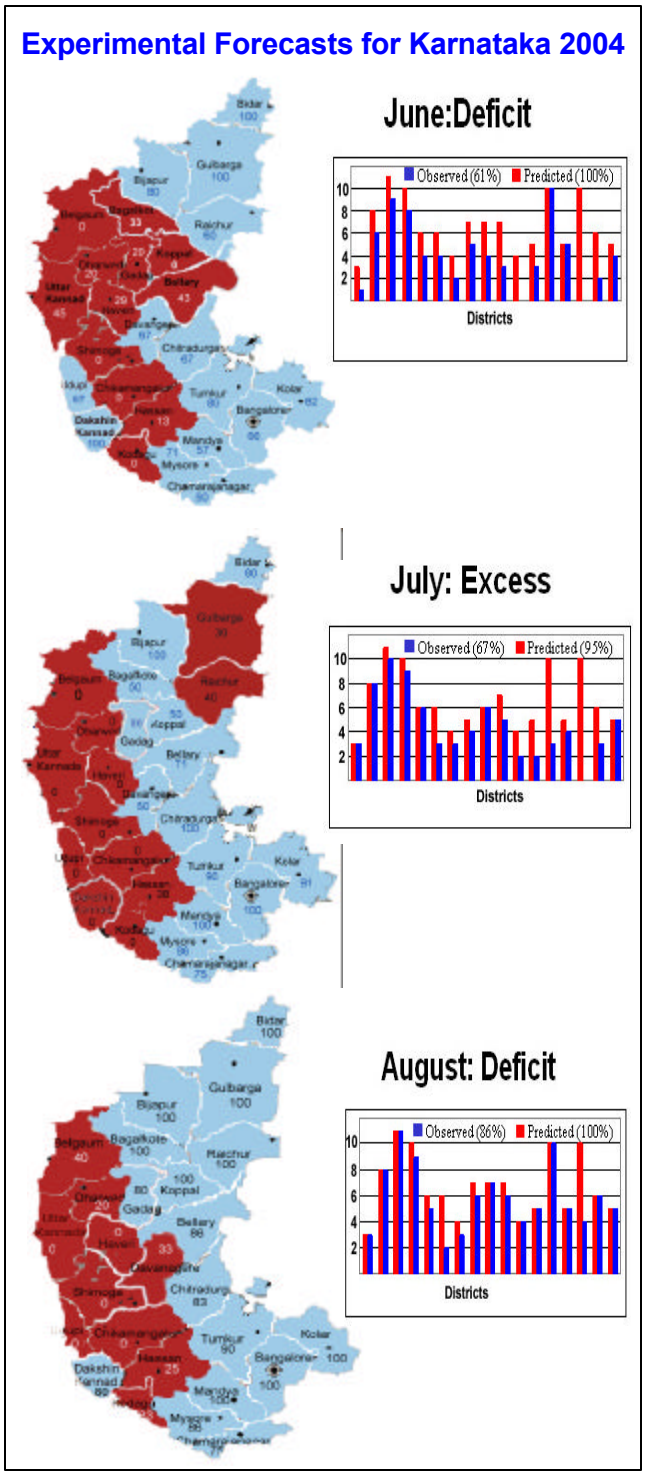

Fig 1.3 District-level map of Karnataka showing performance of C-MMACS experimental forecasts at taluk level. The measure of the performance is the number of taluks (expressed as percentage of total taluks) for each district for which the direction of departure (excess/deficit) is same as that observed. The blue (red) areas are those over which the performance is above 50% (below 50%). The bar diagrams show the number of excess/deficit taluks for each district.

$$h_i = 1 - \frac{N_{f,i} - N_{o,i}}{N_{total,\,i}} \qquad (1)$$

where,

$N_{total\ i}$ = Number of total taluks in the district i

$N_{o,i}$ = Number of excess/deficit taluks observed in district i

$N_{f,i}$ = Number of excess/deficit taluks in forecast for district i

Fig 1.3 shows the performance of the model for three months of June, July and August, 2004 in terms of h. For 2004, June, July and August for Karnataka were, respectively, largely, deficit, excess and deficit.

To begin with, the forecasts had large errors in terms of amplitudes of anomalies (departure from respective mean). However, the forecasts did reasonably well in terms of predicting the directions of the departures (excess/deficit).

An intriguing fact is that the success rate was close to 100% for a number of districts while it was close to zero for a few other districts; the districts over which the model performs poorly are consistently over western sector characterized by sharp orography, land-ocean contrast and dense vegetation. This points to a certain characteristics of the model in terms of its performance over different geographical locations. The overall success of the model is quite satisfactory at taluk level; if such a success rate is sustained in a statistical sense, these forecasts can provide significant input into such critical issues like agricultural planning, fodder banking and power generation.

As mentioned earlier, accurate long-range forecast of rainfall at taluk-level is still akin to a scientific dream. The sucess of the model in this difficult but critical area, though still very limited, is thus encouraging. Greater skill can be expected with higher resolution, better data and improved model physics.

Achintya Mandal, V S Prakash and P Goswami

1.2 Effect of the Variability of Vegetation Fraction on Moist Processes over the Monsoonal Region

The important role played by the hydro-biospheric processes in the evolution of soil moisture, microclimate, meso-scale circulation, local scale precipitation and regional scale monsoon variability are now generally well recognized. It has been reported that high initial soil moisture conditions may in fact delay the onset of precipitation, but increase its amount and may thus lead to high intensity storm activities. Large-scale variation in land surface properties like desertification may lead to decreased precipitation and weakening of tropical easterly jet. Proper representation of these processes is therefore an important aspect of weather and climate forecasts.

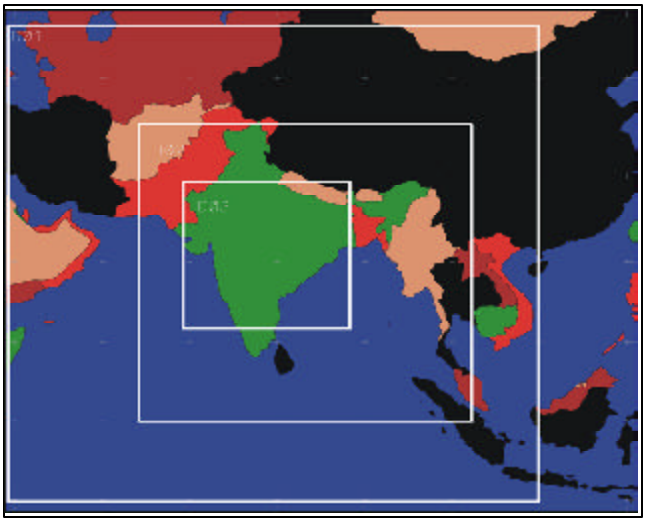

Fig 1.4 Nested Domain of the TERRAIN Model

C-MMACS has initiated a study aimed at investigating the role of vegetation in short-term (a few days) dynamics of moist processes in a mesoscale framework using MM5. The focus of the study was on Relative Humidity (Rh), Total Precipitation (Rc+Rn), Perceptible water (Pwat). Details of model setup and data are shown in Table 1.1. The nested model domain of the TERRAIN is shown in Fig 1.4

MODEL SETUP AND DATA

TERRAIN	MM5	Design of Experiments
3 Nests: 2-way interaction D1 : 80 x 90 x 90 D2 : 142 x 142 x 30 D3 : 211 x 211 x 10 Nest: Two Way LSM: Noah	Vertical Levels : 23(σ) BC : Relaxation Cumulus Scheme: Grell	Vegetation Fraction : 3 Sets IC : 01:08:04:00Hr (NCEP) Forecast Length : 5 days

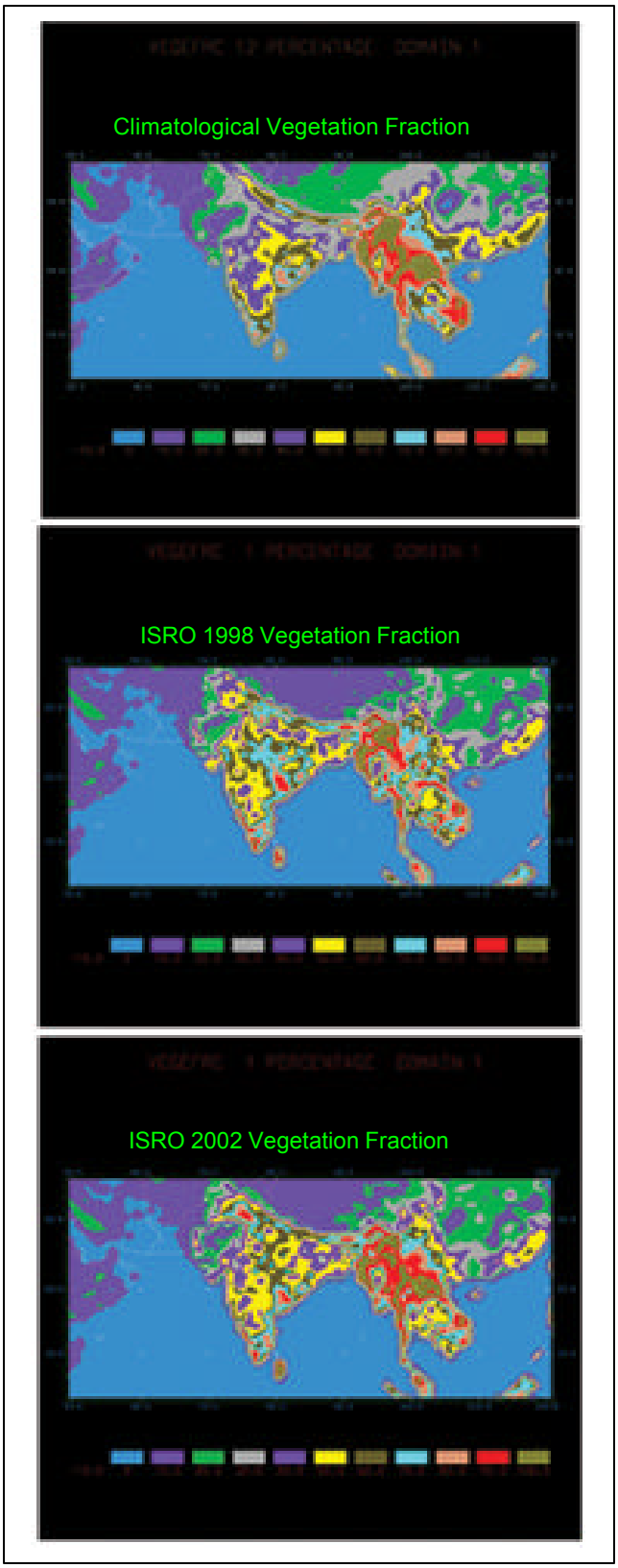

Fig 1.5 Vegetation Fraction 1 for Climatological, ISRO 98 and ISRO-02 Data Sets

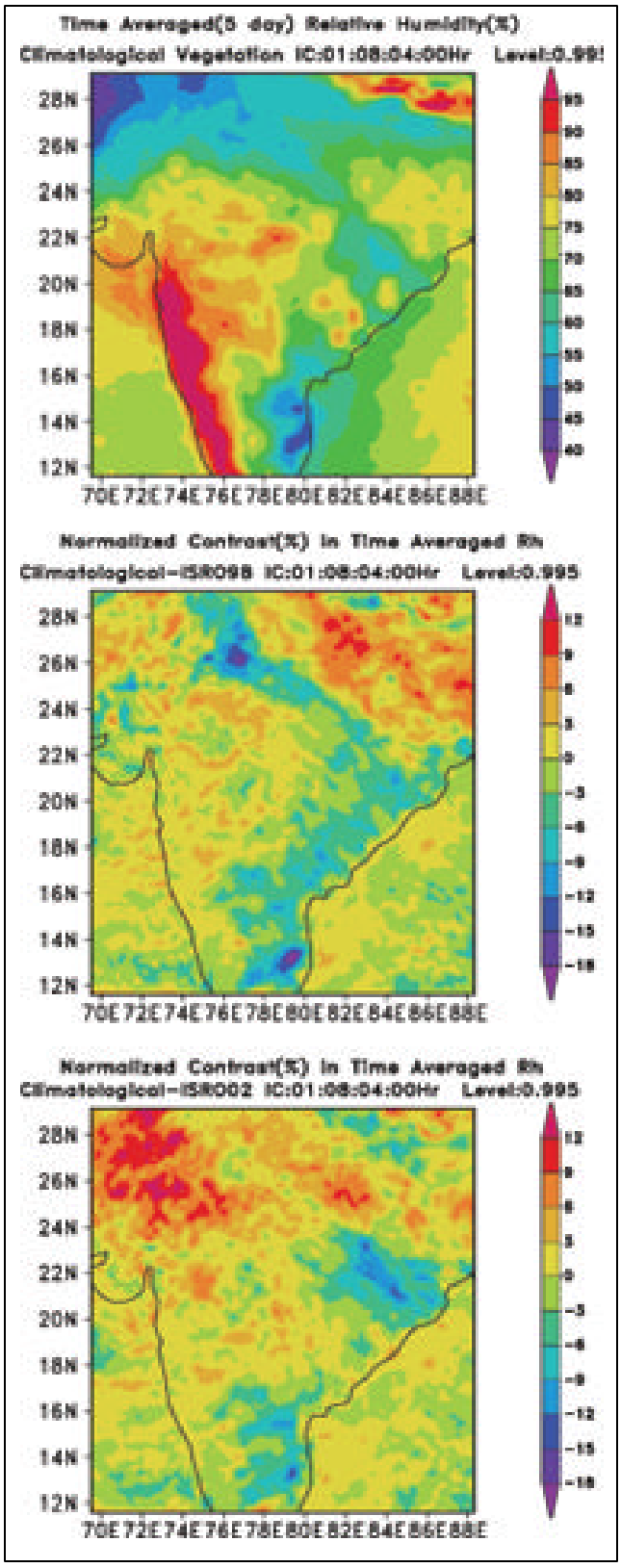

Fig 1.6 Lat-Long Structure of Normalized Contrast (%) in Time Averaged Relative Humidity

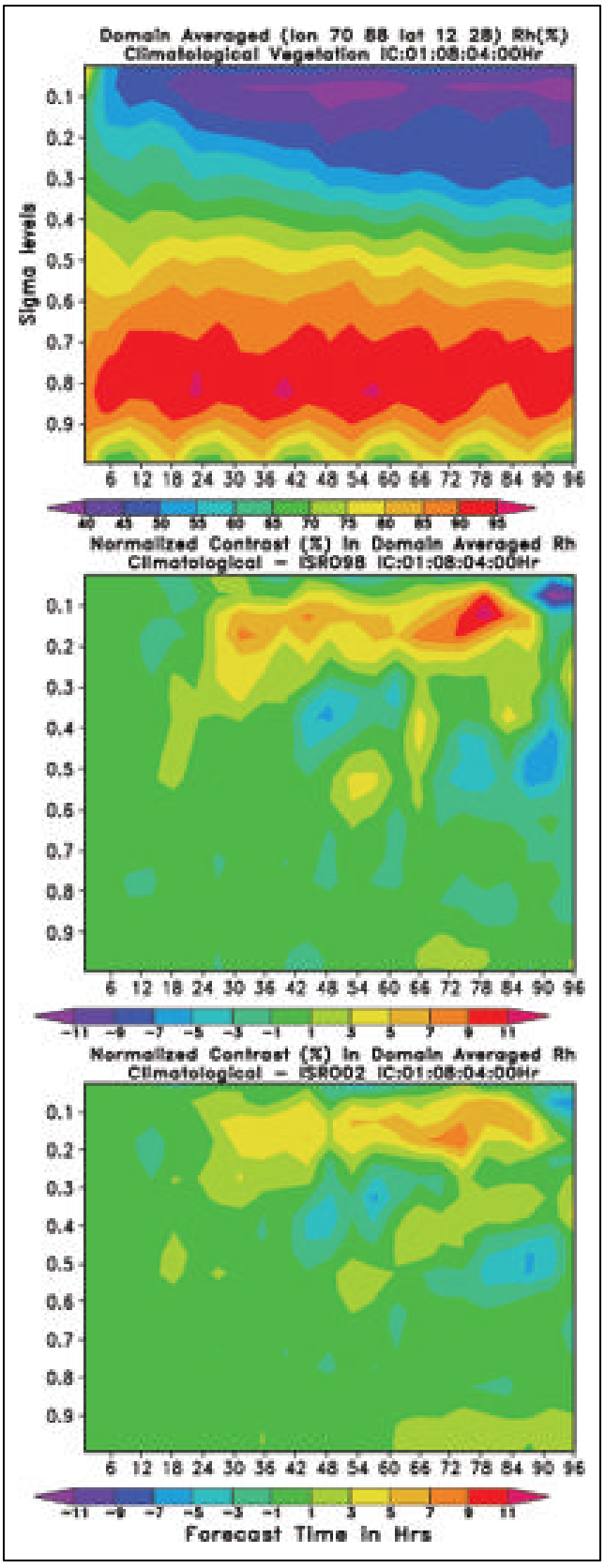

Fig 1.7 Time Evolution of the Vertical structure of Rh (%)

Simulation Scenarios: Control Experiments Integration of MM5 with a Climatological Vegetation Fraction from a given initial condition Sensitivity Experiments; Integration of MM5 with a ISRO Vegetation from a given initial condition.

Climatological, ISRO-98 and ISRO-02 Vegetation Fraction data are shown in Fig.1.5. The simulations revealed significant effect of vegetation on moist process. Normalized contrast (between ISRO and Climatological vegetation fraction) in Relative Humidity varied in the range of -18 to + 12 % (Fig.1.6). Normalized contrast in domain averaged Rh (vertical structure) varied between -11 to 11% for different set of vegetation fraction, as shown in Fig.1.7. These results highlight the importance of proper modelling and inclusion of surface and vegetation processes in short-term forecasting.

S Himesh, Raghu Babu and P Goswami

1.3 Long-range Forecast of Cyclones with C-MMACS CGCM: A Case Study with Bay of Bengal Cyclones

Every year coastlines in many parts of the world face the threat of tropical cyclones. Although there has been significant improvement in areas like observation system and dynamical forecasting, the tropical cyclones in fact are a growing threat due to the increasing economic activities in the coastal areas. There is thus increasing demand for longer range and better accuracy in the forecasts of critical parameters like track and intensity. However, the current skill in track forecasting, even 48 hours in advance, is much below the desired level for most operational centers, with average error in 48-hours forecast of track about 200 Kms. It is clear that more comprehensive modeling of tropical cyclone dynamics is required to improve model performance.

Two major weaknesses in most dynamical tropical cyclone forecasting systems of to-day are: an inadequate representation of scale interaction as most tropical cyclone forecast systems use limited area or meso-scale model and the absence of a comprehensive ocean-atmosphere couple dynamics. In the present work we present a model configuration that addresses these two issues; we then investigate the performance of the model in simulating track and intensity of a number of cyclones over the north Indian Ocean.

The coupled configuration involves an Atmospheric General Circulation Model (AGCM) and an Oceanic General Circulation Model (OGCM). The AGCM is the variable resolution AGCM developed at LMD, Paris. The variable resolution allows relatively high resolution over a domain of interest at a comparatively affordable computing cost.

The AGCM has a 192x144x19 grid set up with zoom over the low pressure area. The initial conditions are from NCEP daily data. The OGCM is the Modular Ocean Model (MOM3) developed at GFDL Princeton, with 180x90x13 uniform horizontal grid and a fine vertical resolution with 5m at the top. The initial conditions for MOM are from Levitus monthly climatology of salinity and temperature. A separate module, using the top layer temperature simulated by MOM calculates the SST fields required for AGCM. The ocean model is forced with daily winds derived by the AGCM.

We have considered the Oct-Nov period for the past 30 years (1971-2000) to examine the models performance in simulation of cyclone over the Bay of Bengal. Each simulation starts with initial condition on Oct 1st of the corresponding year with MOM having a 5-year spin-up before that. Fig 1.8 shows the results for 3 selected years in terms of maximum sustained winds during the Oct-Nov period. Some of the events, like the Orissa super cyclone of 1999 are captured well while some events there is a difference of about 2 days between the observed and the simulated events. The initial perturbations indicate a spin of time of atleast 10 days.

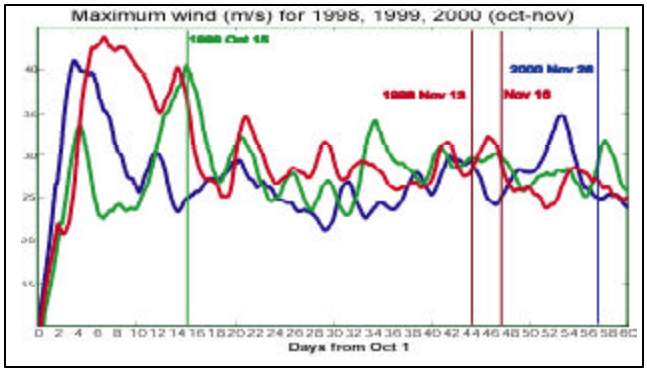

Fig 1.8 Maximum sustained winds over Bay of Bengal for the Oct-Nov period as simulated by the C-MMACS Coupled General Circulation Model. The vertical lines indicates the observed date of occurence of cyclones.

The coupled configuration was used to simulate a number of cyclones over the North Indian Ocean in the past decades. These simulations confirm significant impact of coupled dynamics in track and intensity of tropical cyclones and indicate ocean-atmospheric coupled models as potentially useful tool for advance forecasting of tropical cyclones.

P Rajeevan and P Goswami

1.4 Pre-monsoon Organization of Dynamics as a Predictor for Monsoon Intensity

The precipitation pattern associated with the Indian summer monsoon is a result of a complex interaction among many scales and processes. While the important roles of physical processes like convention and boundary forcing like SST and snow cover in monsoonal precipitation has been well recognized, relatively less attention has been paid to the role of organization of dynamics in determining the structure and intensity of monsoonal precipitation. In our previous work we had shown that there exists a characteristic scale of organization of dynamics (convergence) that plays a critical role in determining monsoon intensity.

Indian Summer Monsoon (ISM) is a large-scale convective system. While the surface heat source that develops due to the seasonal cycle of solar heating initiates the low-level convergence, development of a deep heat source through moist convection is necessary for large-scale precipitation. A mechanism that can play a critical role in this process is convective feedback, leading to scale selection. In a recent study, it was shown by the authors that nature and organization of dynamics play a critical role in the intensity, and hence the variability of ISM. Investigation using a 55-year dataset from NCEP at different scales and locations clearly shows a sharp contrast in organized convergence at a scale of 20° between excess and deficit monsoon years; the deficit monsoon years, including 2002, are marked by suppressed organized convergence. In particular, it was shown that organized convergence acts like a pump to collect moisture and fuel the monsoon engine.

The purpose of the present study is to examine, for the same data set, whether such a pumping begins even before the actual onset of the monsoon or in the early stages of it. The convective organization is characterized and quantified by equation 2:

$$C_{LS} = \frac{1}{s(H_2 - H_1)} \int_{s} \int_{z=H_1}^{H_2} -\left(\frac{\partial u}{\partial x} + \frac{\partial v}{\partial y}\right) dz\, ds \qquad (2)$$

The vertical integral essentially represents up-ward motion through the continuity equation; H_1 and H_2 are taken to be 1000 and 500 mb, respectively. Here *S* represents the domain corresponding to a scale *s*, over which the convective organization is considered. The pre-monsoon organization is calculated using equation 3.

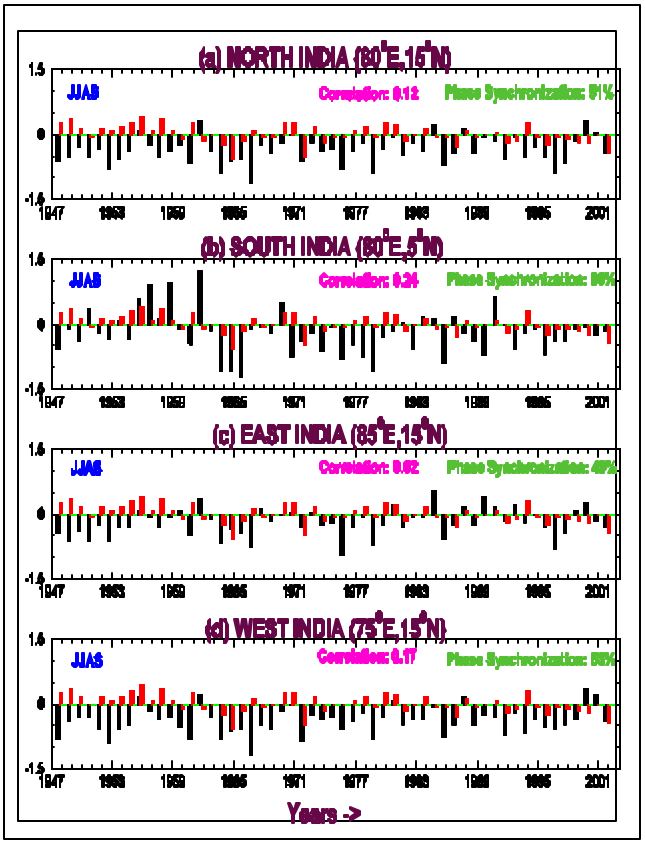

Fig 1.9 Association of May (16-29) convergence with the seasonal Rainfall (JJAS) for different location [(a) North India (b) South India (c) East India (d) West India] at 200 scale from 1948-2002. The RED (-) bar shows the seasonal rainfall anomaly and BLACK (-) bar indicates the late May convergence. The graphs also provide correlation and the percentage phase synchronization between area averaged precipitation (seasonal) and the convergence averaged over 16th to 29th May for 55 years.

$$\overline{C}_{LSM} = \frac{1}{(m_2 - m_1)} \sum_{n=m_1}^{m_2} C_{LS}(n) \qquad (3)$$

Here, m_1 and m_2 are the initial and final day considered for finding the convective organization in the month of May. To associate C_{LSM} and rainfall, the 55 years of NCEP reanalysis precipitation data (R) over rectangular box (70°E-85°E; 10°N-30°N) is considered. Organized convergence averaged for various periods in the second half of May were considered to find out the association with seasonal and monthly rainfalls. It was found (Fig 1.9) that the seasonal monsoon intensity is significantly associated with the pre-monsoon/ early monsoon organization of convergence; the excess (deficit) years are characterized by strong (weak) organization of convergence at about 200 scale over South India. From the association it can be concluded that, it is the trigger provided by the late May convergence, which determines the nature (Excess/Deficit) of monsoon to a large extent. Our results not only provide new insight into the dynamics of monsoon but also provide a novel predictor that can supplement other seasonal prediction parameters. This also provides a viable and novel diagnostic for model evaluation/validation.

G K Patra and P Goswami

1.5 Application of 4D-Var Assimilation to Generate Ensemble Initial Conditions

Ensemble forecasting has emerged as an indispensable tool in meteorological forecasting since its introduction in the early nineties. The basic philosophy of ensemble forecasting is to generate a set of forecasts, such that the average of the ensemble of the forecasts is more accurate than a single deterministic forecast. Besides, the spread in the ensemble contains quantitative information about the reliability of forecasts, and provides a basis for probabilistic forecast. An ensemble forecasting, however, should be able to (non linearly) filter errors for it to be considered good, or useful for forecasting. A critical issue in ensemble forecasting is thus how to create a good ensemble, that is, how to create a set of initial perturbations that would result in a better forecast.

In this work we propose a methodology to generate a set of initial conditions using Four Dimensional Variational assimilation (hereafter 4D-VAR). Instead of considering perturbations to a best estimate as in an ensemble assimilation system, we generate a number of best estimates by taking advantage of certain features of 4D-VAR assimilation system as discussed below. Similarly, the observations are not perturbed, but the number of observations (information) assimilated is slightly varied to generate different estimates; we shall call this informational perturbation to distinguish it from ordinary (random or systematic) perturbation to the fields themselves. The use of 4D-VAR assimilation to generate the estimates ensures that each member is as close an approximation to an allowed model solution as possible, a property unlikely to be shared by a randomly perturbed estimate. As mentioned, this is possible because of the mathematical structure of 4D-VAR assimilation.

The basic principle of 4D-VAR assimilation is to determine X (t=0) that will minimize the gradient of the objective function.

Let us consider an objective function of the form

$$J = \frac{1}{N}\sum_{n=1}^{N}\left|\left(X(n) - X_0(n)\right)\right|^2 \qquad (4)$$

where N represents the total number of discrete observations.

It is clear that a variation in the amount of information, through a variation in N will change J, which, in turn, will change the estimated state, at least in principle. A typical 4D-VAR assimilation experiment is carried out with a given length of assimilation interval or window (hereafter AI) and a given frequency of observations (hereafter OF). While the later is generally constrained by the observation schedule, the former can be varied relatively easily. A change in either AI or in OF would mean a change in N. We may call such a variation an informational perturbation (with respect to a reference initial state) which will affect the corresponding forecasts; for strongly non-linear systems like the atmosphere and the ocean these effects can be significant. A set of 4D-VAR assimilations, with N varied in an optimal range, will thus produce a set of estimates (initial conditions) which are dynamically consistent, with a spread that is also determined in an objective and dynamically consistent manner. We investigate this issue using a representative non-linear system, viz. The Lorenz system with three variables, described by the equations:

$$\begin{aligned} \dot{X}_1 &= a\left(X_2 - X_1\right) \\ \dot{X}_2 &= gX_1 - X_2 - X_1X_3 \\ \dot{X}_3 &= X_1X_2 - b\ z \end{aligned} \qquad (5)$$

where α, β and γ are real, positive parameters. The Lorenz system is highly representative of the atmospheric and oceanic dynamics in terms of its strong sensitivity to initial conditions. It has also been used to investigate generation of initial conditions. It is well known that this system can represent different dynamical regimes depending on the values of the parameters, especially. Table1.2 gives the seven sets of parameters that were considered in this study.

Table 1.2: Values of Parameters for different regimes

Set	Parameters			Dynamical Regime
	α	β	γ	
1	100	27.00	10.60	Chaotic
2	10	23.00	2.66	Non-Chaotic
3	28	46.92	4.00	Chaotic
4	16	40.00	3.66	Chaotic
5	10	13.92	2.66	Non-Chaotic
6	10	24.50	2.66	Chaotic
7	10	28.00	2.66	Chaotic

The 4D-VAR assimilation experiments in the present case were designed as follows: First, 'observations' were created by integrating the Lorenz model from a given initial condition. Next, 4D-VAR assimilation was carried out for a given AI and OF; the AI was changed in steps of 6 time steps up to a maximum of 120 time steps. Although a longer AI implies more (observational) information incorporated into the assimilation cycle, it also implies a longer integration of the model. The latter may offset gain due to the former due to growth of model error; an optimum AI, therefore, has to be chosen for each assimilation system. The OF was

changed between 1-3; for OF=1 an observation is assimilated every step, while for OF=3 an observation is assimilated every third time step. The minimization of the objective function was carried out using a variable- storage quasi-Newtonian algorithm. In general terms, the method uses information from the past iterations to approximate the inverse of the Hessian matrix. The inputs to the minimization algorithm are the objective function J, and the gradient of J with respect to the control variable (initial conditions) which must be computed accurately through the adjoint code. This procedure was carried out for a number of dynamical regimes of Lorenz system, represented in terms of X_1, X_2 and X_3, as shown in Table1.3. For each dynamical regime, a number of realizations of observations were created by adopting different initial conditions; the five initial conditions used in this study are given in Table1.3. In what follows, we shall mostly present results from realization average from these five set of "observations".

Table 1.3 : The set of initial conditions

Set	Variables		
	X_1	X_2	X_3
1	8.53	1.95	32.89
2	5	5	35
3	1	0	1
4	-4.5	0.69	23.9
5	2	5	20

Let $X(i,j)$, i =1,2,3 be the estimate for X_i with the jth 4D-VAR assimilation experiment. We can define the ensemble average initial condition as

$$\overline{X}(i) = \frac{1}{N}\sum_{j=1}^{N} X(i,j) \qquad (6)$$

where N is the size of the ensemble
We can then formally define a perturbation for each i and j as

$$X'(i,j) = X(i,j) - \overline{X}_i \qquad (7)$$

The informationally constructed members of the ensemble can then be formally represented as

$$X_I(i,j) = \overline{X}(i) + X_I'(i,j) \qquad (8)$$

In contrast, the non-informationally constructed (arbitrary) members of the ensemble may be represented as

$$X_A(i,j) = \overline{X}(i) + (r)X_I'(i,j) \qquad (9)$$

where r is a random number between -0.8 and 0.8.In constructing the arbitrary perturbations, it is assumed that the knowledge of the ensemble average is available from previous statistical analysis of the system. The amplitude of the random perturbations are constrained to be <= 0.8 to keep $X_A(i,j)$ close to $X_i(i,j)$ in magnitude.

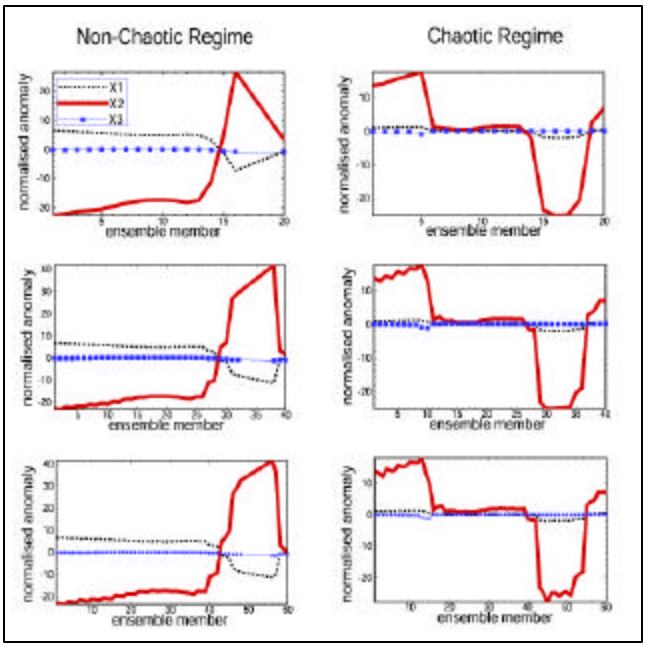

Fig 1.10 Normalized anomaly (as percentage of ensemble mean) for three variables X_1, X_2 and X_3 of Lorenz equation. The left panel is for a non-chaotic regime (α =10, β =23, and γ=2.66) while the right panel is for a chaotic regime (α=28, β=46.92, and γ=4).

Fig 1.10 shows the nature of these perturbations in the three variables in terms of percentage of the ensemble mean for different members of the ensemble (x-axis). The spread in X_3 is rather small (a few percent of the ensemble mean) while the spread in X_2 can be as much as 20% or more of the ensemble mean.

We next evaluate relative performance of informational and arbitrary ensemble forecasting in terms of normalized forecast errors, defined as

$$e_{Ai}(j,t)=\frac{1}{N_e}\sum_{j=1}^{N_e}\left|X_A(i,j)(t)-X_{0i}(t)\right|\times 100/X_{0i}(t) \quad (10)$$

$$e_{Ii}(j,t)=\frac{1}{N_e}\sum_{j=1}^{N_e}\left|X_I(i,j)(t)-X_{0i}(t)\right|\times 100/X_{0i}(t) \quad (11)$$

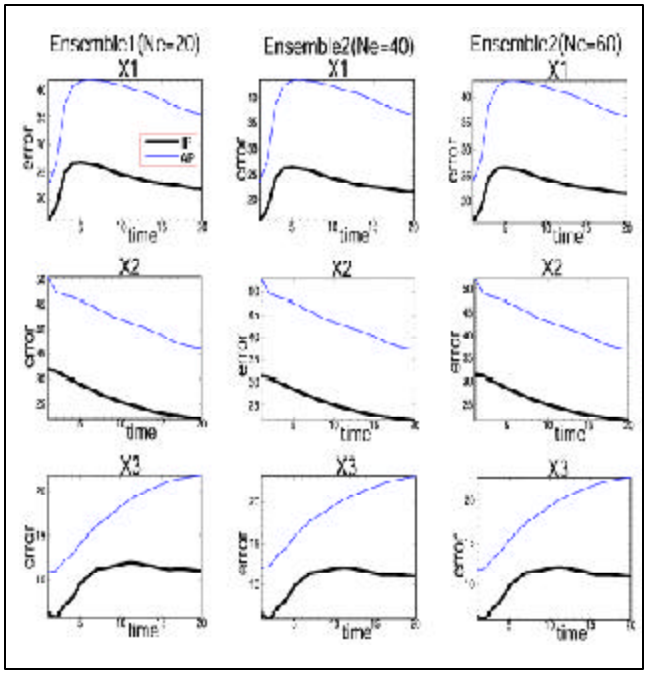

Fig 1.11 Cumulative growth of forecast error as a function of forecast time (integration step) for the three variables of Lorenz equation for informational perturbation, IP (black line) and arbitrary perturbation, AP (blue line). The results represent average of five realization of observations for a chaotic regime (α =100, β=27, and γ=10.66)

Fig 1.11 shows the cumulative forecast error, expressed as percentage of the corresponding observation, for three variables of Lorenz system; the thick line represents result for informational perturbation (IP) while the thin line shows the corresponding results for arbitrary perturbation (AP). The three columns in Fig 1.11 represent three ensembles characterized by, respectively, AI= 20, OF = 1; AI = 20, OF = 2 and AI =20, OF = 3. As mentioned earlier, the results represent average of five realizations of observations obtained by integrating the Lorenz system (for the given regime) with the five initial conditions given in Table 1.3. It is clear that use of IP can significantly reduce forecast error in comparison to AP.

K C Gouda and P Goswami

1.6 Coupling of Mixed Layer Processes and Thermocline Variations in the Arabian Sea

Dynamical interactions between the oceanic mixed layer and the underlying thermocline provide vital information about the mechanisms of ocean heat storage. The present study examines the importance of such interactions in the Northern Indian Ocean, which is predominantly influenced by a unique monsoon cycle characterized by pronounced seasonal wind reversals and well-defined atmospheric forcing regimes. The main objective of this study is to understand the role of the Southwest monsoon circulation in influencing the Arabian Sea response through physical interactions between the mixed layer and the thermocline underneath. In addition, the study also examines the interannual variability of the upper-ocean temperatures in relation to interannual variations of the southwest monsoon circulation. The results are based on an analysis of observed data sets from multiple sources, including observations from a network of Argo floats during (2002 and 2003). Examination of the seasonal cycle of the upper-ocean thermal structure shows that the surface cooling of the Arabian Sea, during the southwest monsoon season, is accompanied by significant warming of the thermocline; the thermocline is warmer by about 1.2°C in the south-central Arabian Sea during the southwest monsoon season relative to other months (Fig 1.12).

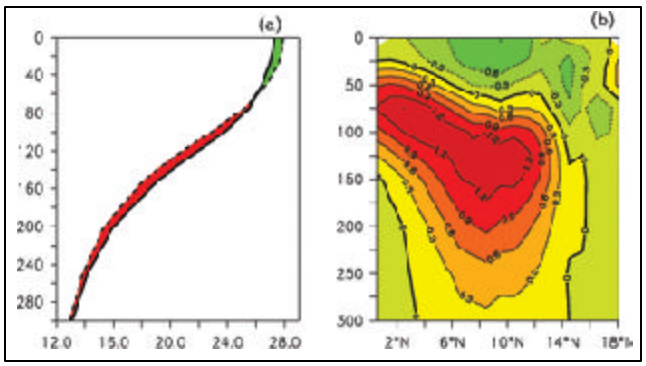

Fig 1.12 (a) Vertical profile of temperature (°C) averaged for the Central Arabian Sea (50°E-70°E;5°N-15°N) based on the WOA2001 dataset. The solid line represents T_{JJAS} and the dashed line corresponds to T_{REST}. The green shading shows the area for which T_{JJAS} is less than T_{REST}. The red shading shows the area for which T_{JJAS} is more than T_{REST}. (b) Latitude-depth section of the (T_{JJAS} - T_{REST}) difference zonally averaged across (50°E-70°E) based on WOA2001.

The monthly climatological values of the oceanic and atmospheric parameters, shown in Fig 1.13, are useful in interpreting the air-sea interactions in the region. The net heat flux variation shows a semi-annual cycle with maxima during the April-May and September-October months; and minima during the December-February and June-July months (Fig 1.13a). On the other hand, the surface wind-stress forcing is strong in the southwest monsoon season which enhances the evaporation from the Arabian Sea. Due to the increased evaporation, the surface density variation (blue line) in Fig 1.13b attains a peak during the Southwest monsoon season. It can be clearly seen from Fig 1.13b that the density stratification (vertical density gradient Δr) in the vertical is very weak during the South-west monsoon season. In contrast, the vertical density stratification is strongest during late spring.

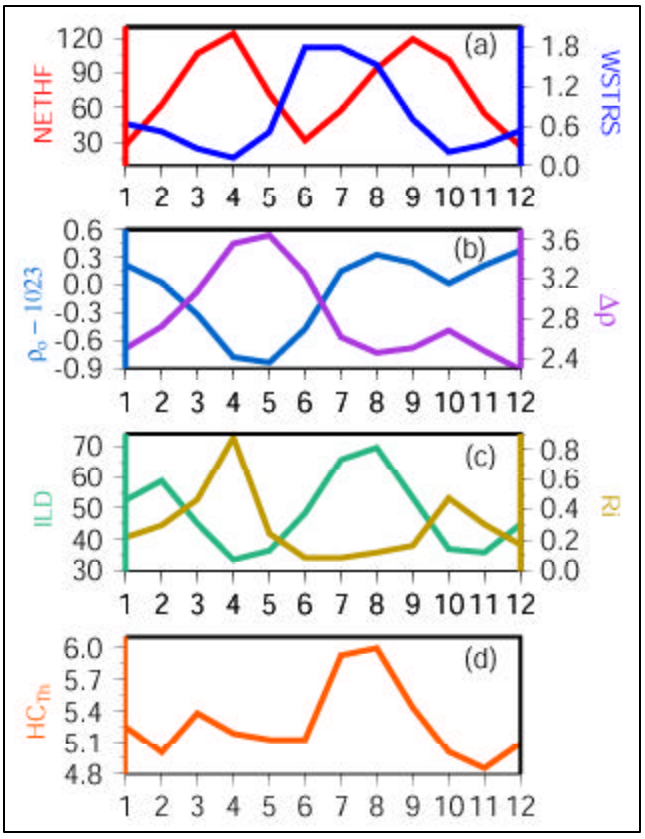

Fig 1.13 Monthly time-series of atmospheric and oceanic parameters averaged for the region (50°E-70°E; 0-20°N) as indicated (a) Net-heat flux (red) in Wm^{-2} and magnitude of surface wind-stress (blue) in dynes cm^{-2}. (b) Surface density in kgm^{-3} (light blue) after subtracting a reference value of 1023 kgm^{-3}; density difference ($\Delta\rho$) in kgm^{3} between surface and 20° isotherm (purple). (c) ILD (0.8 °C) in meters is shown by green line; and Richardson Number is shown by golden yellow line. (d) Heat storage in the thermocline (HC_{Th}) in Joules m^{-3}.

The combined effects of the wind-stress (Fig 1.13a) and the density stratification (Fig 1.13b) forcing can be inferred from the seasonal variation of the Richardson Number

$$(Ri = \frac{gh\,\Delta r}{r_0 u_*^2}\text{; where } u_* = \sqrt{\frac{t}{r_o}}$$ is the friction velocity; τ is the magnitude of surface wind-stress) shown in Fig 1.13c (golden yellow line). The non-dimensional parameter **Ri** is a ratio of the buoyancy forcing versus the rate of production of shear turbulent kinetic energy. It can be noticed from Fig 1.13c that **Ri** drops to a minimum value lower than 0.25 (critical value for shear instability) during the Southwest monsoon season, indicating the unstable structure of the upper-ocean. In the subsequent discussions, it will be seen that the strong monsoonal wind-driven mixing is accompanied by strong vertical diffusion of heat from the mixed layer into the thermocline. The seasonal variation of HC_{Th} (Joules m^{-3})

$$HC_{Th} = \frac{r_o C_p}{(300 - MLD)}\left(\int_{z=0}^{300} Tdz - \int_{z=0}^{300} Tdz\right)$$

averaged for the Arabian Sea (50°E - 70°E; 0 - 20°N) is shown in Fig 1.13d. Clearly it can seen that HC_{Th} attains a maximum value of about 6.0×10^{10} Joules m^{-3} during July and August months. The value of HC_{Th} averaged from June to September is around 5.74×10^{10} Joules m^{-3}; and the value for rest of the year (all months other than the South-west monsoon season) is found to be around 5.11×10^{10} Joules m^{-3}. Thus the increase in HC_{Th} by about 0.63×10^{10} Joules m^{-3} indicates greater heat storage in the thermocline during the Southwest monsoon season as compared to other months. The results demonstrate that the combined effects of strong wind-driven mixing by the monsoonal winds, weak density stratification in the upper-ocean, and downwelling in south-central Arabian Sea, along with strong vertical diffusivity, favor downward transfer of warm waters from the surface into the thermocline.

Given the seasonal mixed layer cooling and thermocline warming during the South-west monsoon season, we have further examined the changes in the oceanic response due to interannual variations in the monsoonal forcing.

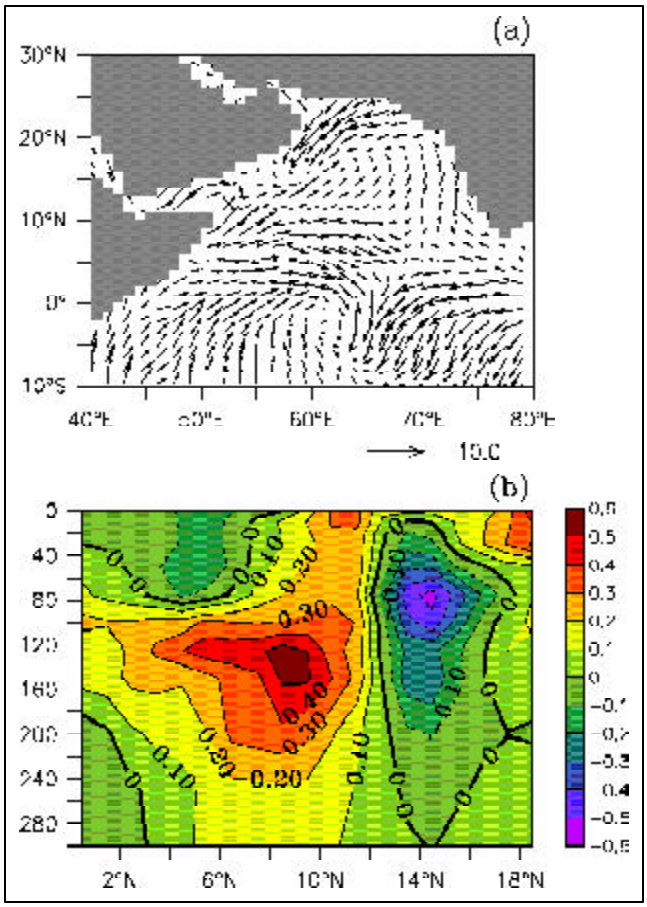

Fig 1.14 (a) Surface wind difference (July 2003 minus July 2002) in ms^{-1} based on QuikSCAT dataset. (b) Latitude-depth section of temperature difference (July 2003 minus July 2002) zonally averaged across (50^0E-70^0E) based on DINDOCN dataset.

Using the long-term ocean temperature data from Joint Environmental Data Archive Center (JEDAC) for the period (1955-2001), we have analyzed the interannual variability in the ocean response associated with strong and weak monsoons. The subsurface anomalies for the strong (weak) monsoon composite indicate anomalous warming (cooling) in the South-Central Arabian Sea by as much as +0.5°C (-0.5°C). In the Northern Arabian Sea, near the coasts of Oman and Arabia, the temperature changes during strong (weak) monsoon years reveal anomalous cooling (warming) due to increased (decreased) coastal upwelling. Furthermore, the isothermal layer depth (ILD) anomalies in the Northern Arabian Sea, for the strong (weak) monsoon cases show an increase (decrease) in the ILD of about 6-8 m, and are found to be out-of-phase with those in the South-Central Arabian Sea. It is found that the interannual variations in the ocean response reveal signatures of the influence of strong and weak southwest monsoons on the mixed layer and thermocline variability.

K V Ramesh and R Krishnan

1.7 Mathematical Modelling of Biogeochemical Cycles in the Indian Ocean

Marine biogeochemical cycles play a significant role in the key environmental issues like, oceanic response to climate change, coastal eutrophication etc. To understand the present ocean biogeochemical state and predict the future responses of the ocean to anthropogenic perturbations, existing mathematical models need improvements. The major challenges in the marine biogeochemical modelling are the identification of the ecosystem compartments, underlying biogeochemical processes and their parametrizations, the model-data comparisons and data assimilation studies.

The process of nutrient uptake by phytoplankton in a multinutrient environment is an important process in the marine biogeochemical cycle studies. A comparative study of the effect of six nutrient interaction laws (Wroblewski-WB, Walsh-WL, Parker-PA, O'Neill-ON, Yajnik & Sharada-YS and Jamat-JA) including a new general formulation (YS - based on the properties of similarity and hyperbolicity which were observed in the experiments), on the dynamics of a seven component marine ecosystem model for the mixed layer was done. The model simulations were carried out for two sets of parameter values for the six kinetic relations and at two stations in the Arabian Sea. These simulations used climatological forcings for the mixed layer depth, solar radiation and subsurface nitrate concentration.

Annual averages of all state variables and fluxes show that almost all the variables and fluxes depend on the choice of model parameters and the location at which model simulations are carried out. Annual averages of almost all state variables and fluxes are minimum for YS relation for both sets of parameters and at both locations. Maximum values of Ammonium and f-ratio are obtained for ON

relation, since regenerated production is much less than new production. For all relations, for two sets of parameter values and at both locations, it was seen from the tables of annual averages that the ammonium regenerated by zooplankton is much more than that due to bacteria, dissolved organic nitrogen is the preferred food for bacteria compared to ammonium, grazing by zooplankton on phytoplankton is greater compared to that on bacteria and detritus, mortality of phytoplankton is greater than that of zooplankton, dissolved organic nitrogen produced by phytoplankton is lower compared to zooplankton and detritus, and the new production, export flux and nitrate input are equal in magnitude. It can be concluded from these studies that zooplankton has significant control on the phytoplankton biomass and the availability of ammonium.

This kind of study helps in selecting the appropriate relation for nutrient uptake kinetics and the corresponding model parameter values, to be incorporated in the three dimensional coupled physical-biological model for the Indian Ocean.

As a part of marine biogeochemical modelling studies under Bay of Bengal Process Studies (BOBPS) Programme, 3D simulations of coupled physical-biological-chemical model were performed at C-MMACS to understand the effect of the formulation of uptake by phytoplankton in two-nutrient environment on the dynamics of marine ecosystem, the influence of the values of model parameters on biology and chemistry of the ocean and the effect of biological processes on the carbon flux across the ocean surface.

To determine the role of the biological pump, two types of simulations were carried out - abiotic (coupled physical-chemical model) and biotic (coupled physical-biological-chemical model). One set of parameter values for biological model (basic experiment) was chosen as the most appropriate for the biotic simulations and a detailed analysis of the spatial and seasonal variation of all the tracers was done. Since the results of this simulation showed that pCO_2 at the surface for biotic simulations are more than that of abiotic simulations for all seasons, on two transects, one each in Arabian Sea (AS) and Bay of Bengal (BOB), which is contrary to the expectations, a question arose whether the parameter values were responsible for these counter intuitive simulation results. It was seen that the values of primary productivity and chlorophyll obtained from the basic experiment compared well with the US JGOFS observations at a few locations in AS and also with SeaWiFS data, but the concentrations of Ammonium and Zooplankton obtained from this model simulation were very high compared to the observations, which were contributing to the high values of dissolved inorganic carbon or pCO_2. Therefore, a detailed study of the source and sink terms of the tracers Dissolved Inorganic Carbon (DIC) and Alkalinity (ALK) and sensitivity of the parameters related to the regeneration of Ammonium (or DIC) by zooplankton and bacteria, and grazing by zooplankton to the ecosystem dynamics and carbon flux was carried out.

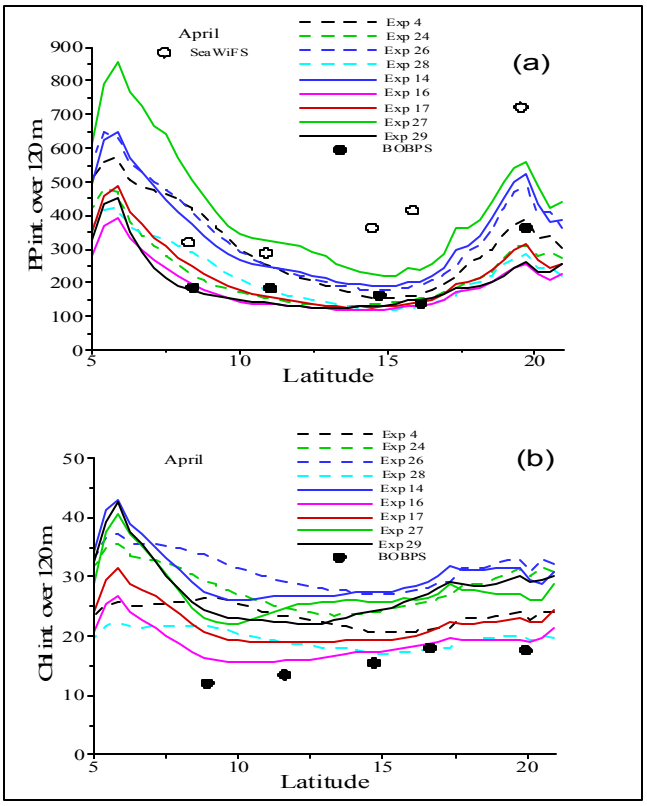

Fig 1.15 (a) Depth integrated PP (mg C/m^2/day) values from different model simulations compared with the BOBPS data and SeaWiFS data during SIM. (b) Depth integrated Chl values (mg Chl/m^2) from different model simulations compared with the BOBPS data during SIM.

Several numerical experiments for the coupled physical-biological and physical-biological-chemical model were carried out using the YS relation for nitrate uptake and by varying the parameters influencing the zooplankton grazing and regeneration of ammonium by zooplankton and bacteria.

Detailed analysis of fluxes and concentrations of tracers was carried out for two numerical experiments, namely, basic experiment (standard set of parameter values) and a particular numerical experiment (selected experiment) which yielded the minimum zooplankton and ammonium concentration. The latitudinal variation of depth integrated values of Primary Productivity (PP) for three seasons on 88^0 E transect from the selected experiment compares well with cruise data of BOBPS and SeaWiFS data, but the depth integrated values of chlorophyll obtained from selected experiment are always much greater than that of the cruise data (Fig 1.16).

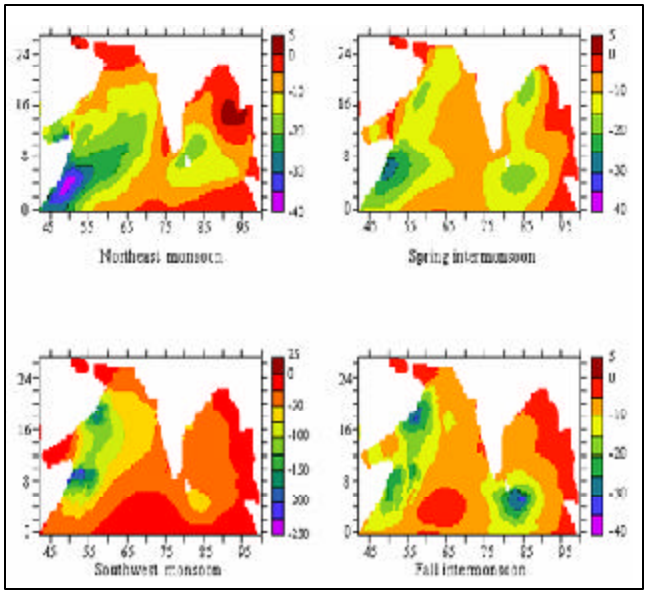

Fig 1.16 Spatial and temporal variation of surface Carbon flux (g C/m^2/year) from atmosphere to ocean obtained from model simulation (Selected Experiment -exp29).

Chlorophyll, Primary Productivity, DIC, ALK, pCO_2 in BOB are found to be less than those in AS for both numerical experiments. Hence the carbon flux from ocean to atmosphere is lower in BOB. The spatial and temporal variation of carbon flux obtained from model simulations (selected experiment) shows behaviour similar to the climatological data set of Takahashi et al. (1999) which is available on 4^ox5^o grid. Carbon flux values obtained from model simulations are higher than the climatological data (Fig 1.16). pCO_2 at the surface from the model simulations is comparable with the values available from the BOBPS cruise for one season.

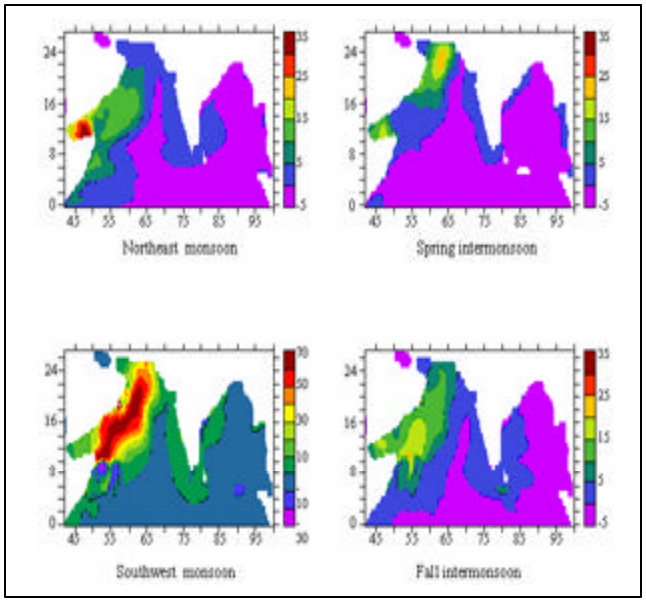

Fig 1.17 Spatial and temporal variation of difference in carbon flux (g C/m^2/year) for the selected experiment and abiotic simulations

The simulation results of the selected experiment show that biology reduces the outgassing (Fig 1.17). AS and BOB are sources of carbon for both biotic and abiotic experiments during all seasons. Abiotic carbon flux from ocean to atmosphere is less than biotic for the basic experiment and abiotic carbon flux from ocean to atmosphere is more than biotic for the selected experiment at regions where primary productivity is high. These numerical experiments carried out using different sets of parameter values show that the estimate of carbon flux across the surface of the ocean is influenced to a great extent by the parameter values used for simulations. This study helps in understanding and quantifying the various processes of carbon cycle and climate change.

P S Swathi, M K Sharada,K S Yajnik, and Kalyani Devasena

1.8 Use of an Atmospheric Chemical Tracer Model for Carbon Flux Studies

With a growing concern related to the influence of greenhouse gases like carbon dioxide, methane etc., on the climate system of the earth, it is being recognized that it is equally important to study their sources/sinks. Given some estimate of source/ sinks of chemically inert species like CO_2, an atmospheric chemical tracer model (CTM) can simulate the resulting concentration of these species in the atmosphere. Combining this information along with the station observations in an inverse modelling framework will give information on the source/sink estimates of the species. In this project we have implemented MOZART (Model for Ozone And Related Tracers) version 2.4 CTM on Altix computer. Though MOZART has options to include chemical reactions, we are using it as a pure tracer transport model at present mainly for carbon flux studies.

MOZART requires meteorological inputs such as wind, temperature, etc., at regular time intervals. Minimum meteorological data required are three dimensional wind, temperature, specific humidity, two dimensional (surface) latent heat flux, sensible heat flux, skin temperature, zonal and meridional wind stress components, surface geopotential, and land sea flag. If only zonal and meridional components of wind vector are supplied, vertical wind component is diagnosed within the model. MOZART uses a flux form semi-Lagrangian advection scheme with pressure fixer for the large scale transport of the constituents and various subgrid scale parameterizations for convection, atmospheric boundary layer etc. MOZART can be driven with the above mentioned meteorological data at any horizontal resolution while the maximum number of vertical levels are limited to that of the input meteorological data. At present we are using National Centre for Environment Prediction/National Centre for Atmospheric Research (NCEP/NCAR) reanalysis data at T42 horizontal resolution (roughly 2.80 X 2.80 grid cells) and 28 vertical levels in sigma coordinates at 6 hourly intervals, and time step of 20 minutes. We used the 1996 NCEP/NCAR reanalysis in the present set up. The carbon surface flux estimates are taken from Transcom3 protocol. The surface flux estimates for fossil fuel 1990, 1995, neutral biosphere, and oceanic exchange fluxes are prescribed in MOZART and run as four separate tracers. Of these fossil fuel components do not have any seasonality and oceanic exchange fluxes exhibit slight seasonality. Neutral biosphere fluxes contain strong seasonality. The entire globe is divided in to 11 land and 11 ocean regions. A flux with predetermined spatial structure amounting to annual total of 1 Gt carbon is allocated to each of these regions (known as unit basis functions) for which carbon source/sink estimates are to be inferred using inverse modelling.

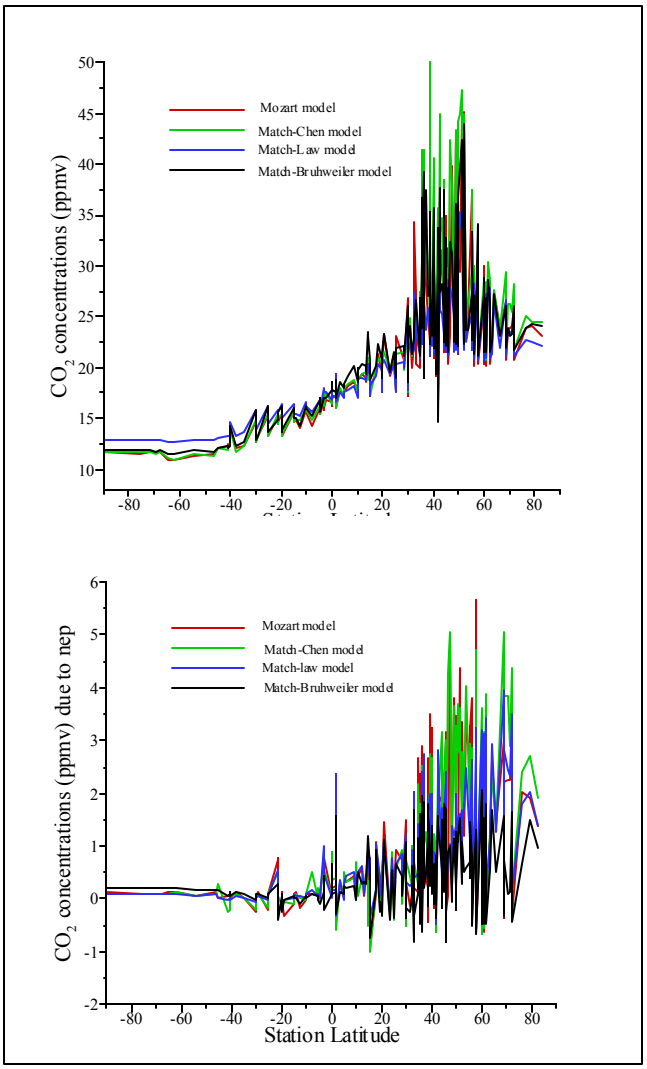

Fig 1.18 Annual mean CO_2 concentration (ppmv) at station locations resulting from all prior fluxes (top panel) and biospheric exchange flux (bottom panel) in 4th year of MOZART and three versions of MATCH model simulations.

Thus we have 26 (four prior estimates plus 22 basis functions) tagged carbon tracers to be transported in MOZART for annual mean carbon flux inversion. We integrated MOZART for four years with NCEP/NCAR 1996 meteorological data repeating for each year (cyclo-stationary dynamic input) with these fluxes and a back ground initial CO_2 concentration of 350 ppmv for all the tracers.

The last year of the four year MOZART simulation mentioned above is used for inverse modelling of annual mean carbon flux estimates. We did a comparison of station CO_2 concentrations resulting from the estimated fluxes with three MATCH (Model for Atmospheric Transport and Chemistry) model integrations. MOZART may be considered a close variant of MATCH. The MATCH results compared here use three different configurations which differ in terms of input meteorology, advection and some subgrid scale parameterizations. Fig 1.18 shows CO_2 concentrations resulting from all the prior fluxes (top panel) and biosphere only (bottom panel) in MOZART and MATCH models. It may be seen that all the models agree very closely. The so called "rectifier effect" in the nep results are also quite similar (bottom panel). Currently we are examining the inverted annual mean CO_2 fluxes in the MOZART model and analyzing the possible sources of uncertainty. Future plans include MOZART simulations to do time dependent carbon flux inversion and to study inter-annual variability in carbon fluxes.

D Jagadheesha, N K Indira, P S Swathi and V K Gaur